Desalination and Water Treatment
www.deswater.com
doi: 10.5004/dwt.2021.26516

211 (2021) 123–130
January

Study of kinetic models of olive oil mill wastewater treatment using electrocoagulation process

Mina Ghahrchi, Abbas Rezaee*, Amir Adibzadeh

Department of Environmental Health, Faculty of Medical Sciences, Tarbiat Modares University, Tehran, Iran, Tel./Fax: +98 2182883575; emails: rezaee@modares.ac.ir (A. Rezaee), m.ghahrechi69@modares.ac.ir (M. Ghahrchi), a.adibzadeh@modares.ac.ir (A. Adibzadeh)

Received 19 January 2020; Accepted 28 August 2020

ABSTRACT

This study investigates the kinetic model of chemical oxygen demand (COD) removal from olive oil mill synthetic wastewater through electrocoagulation using stainless steel and aluminum as a cathode and anode electrodes, respectively. The one-factor method was used to evaluate interactions between the operational parameters that affect COD removal. A reactor with a volume of 250 mL was utilized to perform the process. The optimal conditions with 99% COD were found to be the current density of 12.5 mA cm^{-2}, 400 mg L^{-1} NaCl as supporting electrolyte, initial COD concentration of 17,500 mg L^{-1}, and operation time of 60 min. The highest efficiencies of COD removal were achieved at pH values of 5 and 9 using stainless steel and aluminum electrodes as cathode and anode, respectively. The results demonstrated a direct relation between the coagulant adsorption rate and efficiency of COD removal by olive oil. According to the obtained results, the process follows an intra-particle diffusion kinetic model, in which absorption capacity is high at the beginning, and removal efficiency increases over time.

Keywords: Wastewater; Electrocoagulation; Olive oil; Kinetic; Intra-particle diffusion

1. Introduction

Some wastewaters contain various types of fat, oil, and grease (FOG) that are harmful to nature and the environment. With the rapid industrial and urbanization development, large amounts of FOG are generated by industries such as refineries, petrochemicals, food processing, textile, and leather, which are emitted into the aquatic environment [1,2]. Oily wastewater causes the formation of surface films that affect, ecological resources, surface and groundwater sources, aquatic systems, and human health. Due to the low biodegradability of oil in a natural ecosystem, it is necessary to remove oil from wastewater before discharging it to the environment [3,4]. The common methods such as gravity separation, cyclone separation, chemical precipitation, sorption, membrane filtration, electrocoagulation (EC), and chemical oxidation have been proposed for oil removal [1–5]. Among the proposed techniques, EC is an emerging technology in the treatment of water and wastewater, which is based on destabilization and neutralization of the repulsive forces that help the suspension of particles in water [6,7]. The main advantageous feature of EC, as compared to the method of chemical coagulation/flocculation, is the generation of coagulants by the electrolytic oxidation of an appropriate anode and less sludge generation [8,9]. In the EC process, the anode electrode is dissolved and metal ions as a coagulant are produced. Coagulant in the form of metal hydroxide has a high adsorption capacity. However, the production of hydrogen gases at the cathode could create a large surface area for adsorption flocks and move the flock to the surface [8].

* Corresponding author.

Generally, two separate processes take place in EC: (i) generation of metal flocks and (ii) adsorption of pollutants to the flocks. The scarification of anode produces the flocks. The number of flocks could be estimated by Faraday's Law and stoichiometrically. In the EC process, the insoluble metal hydroxides remove pollutants by surface adsorption. Various kinetic models have been presented for adsorption in the EC process. Fitting of kinetics data with the proposed models can present the mechanism of adsorption [10,11].

2. Experimental procedure

Sodium dodecyl sulfate (SDS) was used to prepare emulsified olive oil wastewater (EOW). Briefly, the EOW was prepared by adding 2 g SDS to 5 mL olive oil in 1 L of distilled water. The chemical oxygen demand (COD) and pH of EOW were obtained as 17,500 mg L^{-1} and 7.0 ± 0.05, respectively. All chemical reagents that were used in the experiments were of analytical grade.

2.1. Experimental setup and analysis

A 0.25 L glass batch reactor with a 7 cm diameter and 6 cm height was used for the coagulation/electro-flotation process (EC/EF) (Fig. 1). Stainless steel (304 L) and aluminum were applied as cathode and anode with 40 cm^2 effective surface area, respectively. The distance between electrodes was 1 cm. A magnetic stirrer was used for aqueous mixing. A direct current (DC) power supply was applied to supply the induced current to the electrodes (APS3005S-3D model, Atten, China). The sodium chloride was selected as a supporting electrolyte. Various concentrations of NaCl (100–500 mg L^{-1}) were evaluated in the experiments. The COD analysis was conducted according to standard methods for the evaluation of water and wastewater. The COD was quantified by a spectrophotometer (Unico-UV 2100, China) at 600 nm. Adsorption capacity, COD removal, current efficiency, and energy consumption were calculated through equations (1–4), respectively [12–15]:

$$\text{Adsorption capacity}\left(\text{mg g}^{-1}\right)=\left[\left(C_0-C_t\right)W\right]\text{m}^{-1} \quad (1)$$

$$\text{COD removal}\left(\%\right)=\left[\frac{\left(C_0-C_e\right)}{C_0}\right]\times 100 \quad (2)$$

$$\text{Current efficiency}=\frac{\left[\left(\text{COD}_0-\text{COD}_t\right)\right]\cdot FV}{8I\Delta t} \quad (3)$$

$$\text{Energy consumption}\left(\text{EC}\right)\left(\text{kwh/m}^3\right)=\frac{\left(V'\times I\times t\right)}{\left(W\times 1{,}000\right)} \quad (4)$$

where C_0 and C_t are initial and final concentrations (in Eqs. (2) and (3): mg L^{-1} and in Eq. (4): g L^{-1}) after treatment time (t), respectively, W is the volume of wastewater (m^3), m is the weight of dissolved electrode (g), F is the Faraday's constant (26.8 Ah), V is the volume of the treated wastewater (L), I is current (A), Δt is reaction time (min), and in Eq. (5), V' is the voltage (volt) and t is reaction time (h).

Experiments were performed in duplicate to ensure the reproducibility of the results. The mean of two measurements was used for representing each evaluation. Current density, pH values, retention time, and supporting electrolytes were investigated for the evaluation of olive oil wastewater treatment. After each experiment, COD, pH, anode corrosion rate, and the amount of power consumption were determined. Kinetic studies were performed using the related models and equations. To determine adsorption kinetics, three simplified kinetics models including the pseudo-first-order, pseudo-second-order, and IPD were evaluated [16,17].

3. Results and discussion

In this study, treatment of olive oil wastewater was studied by EC/EF process using stainless steel and aluminum as a cathode and anode electrodes, respectively. The optimum conditions were achieved for the treatment process. The reaction kinetics and amounts of energy consumption were evaluated at optimum conditions.

3.1. Effect of current

The current intensity in the EC/EF process is the main factor that is effective on the efficiency of COD removal. Olive oil removal efficiency is calculated using Eq. (3). By increasing current intensity, the COD removal efficiency was also increased (Fig. 2). The highest efficiency of removal was obtained at 500 mA current. In the optimum current, COD values were in the range of environmental standards. Increasing the current density could intensify the corrosion and consumption of energy (Fig. 3). Applying the EC processes for the treatment of wastewater by an aluminum electrode in a factory of olive oil extraction showed that the efficiency of COD removal was enhanced using higher current densities [18]. Our findings are in agreement with some scientific reports. Stainless steel electrodes in 100 and 200 mA indicated low corrosion rates and lower COD removal efficiency. Above 300 mA, corrosion rate and efficiency of COD removal exhibited a significant upward trend. However, the aluminum electrode was uniform, uptrends until the current density of 12.5 mA cm^{-2}, and shows some

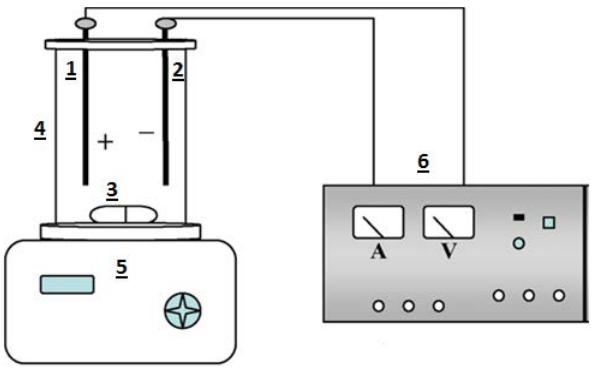

Fig. 1. Experimental setup for the EC process; (1) anode; (2) cathode; (3) magnet; (4) batch reactor; (5) magnetic stirrer; and (6) DC power supply.

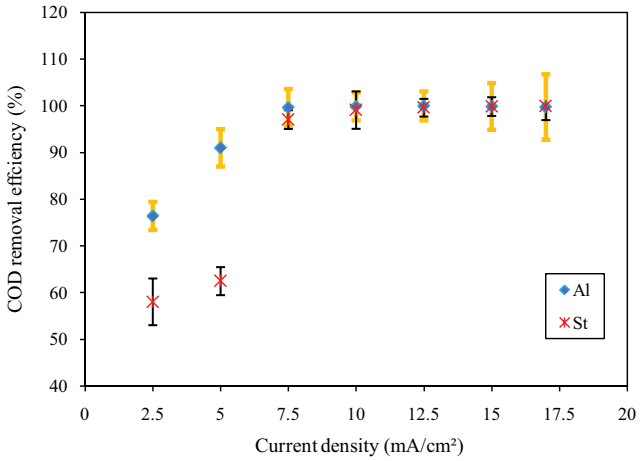

Fig. 2. COD removal efficiency at different current densities (NaCl: 200 mg L^{-1}, pH: 7, and reaction time: 60 min).

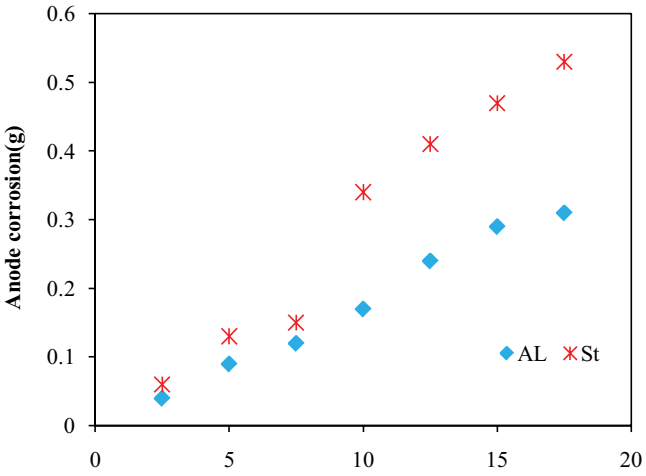

Fig. 3. Anode corrosion at different current densities (NaCl: 200 mg L^{-1}, pH: 7, and reaction time: 60 min).

desorption coagulant and decreasing removal efficiency. The amount of electrical energy applied for the wastewater treatment was calculated based on Eq. (5) [15]. The results show that an increase in the current leads to an increase in voltage and electrical energy consumption. In this regard, it has been proposed an EC method using aluminum and iron electrodes for treating olive oil wastewater [18]. The results demonstrated that energy consumption increases with the current increase. They reported that under the same reaction conditions, the consumption of electrical energy by aluminum exceeds that of the iron electrode. In the present study, energy consumption was increased at greater applied currents.

3.2. Effect of pH

The pH is one of the important parameters that influencing in the EC process. Generally, each pollutant is removed at a specific pH [19]. Fig. 4 shows the impact of pH on the efficiency of COD removal. The experiments were

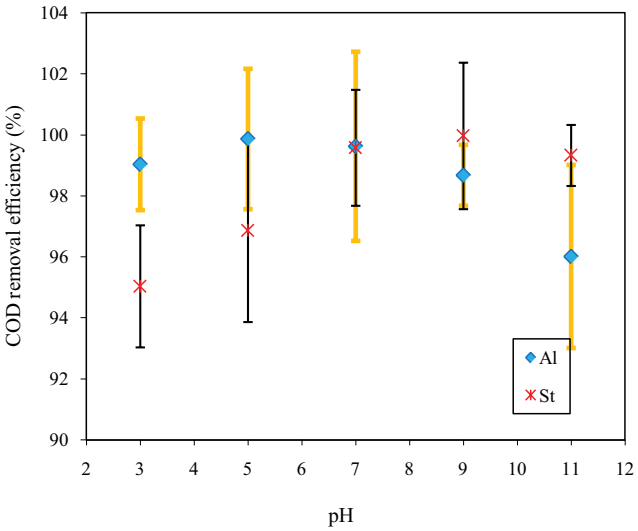

Fig. 4. COD removal rates at different pH values (current density: 12.5 mA cm^{-2}, NaCl: 200 mg L^{-1}, and reaction time: 60 min).

conducted using a current intensity of 500 mA, the reaction time of 60 min, and a supporting electrolyte of 200 mg L^{-1}. The highest removal efficiency by the aluminum electrode (pH = 6) and a stainless steel electrode (pH = 9) was reported to be 52% and 47%, respectively [18]. The results of this study outline 99.86% and 99.96% as the highest removal efficiency by the aluminum (pH = 5) and steel (pH = 9) electrodes, respectively. However, due to the difference in the efficiency of COD removal, at the mentioned pH value compared to neutral pH, pH = 7 was selected as the optimal pH for both electrodes.

3.3. Effect of supporting electrolyte

In this study, sodium chloride was selected as the supporting electrolyte. The supporting electrolyte is easy to access, abundance, and high solubility [19]. The obtained results showed that increasing the supporting electrolyte could lead to an increase in removal efficiency. The highest removal efficiency using 400 mg L^{-1} supporting electrolyte was obtained at 99.5% and 99.77% for steel and aluminum electrodes, respectively (Fig. 5).

3.4. Effect of reaction time

In this study, in the reaction times of 15–67 min were evaluated the COD removal efficiency and current efficiency at a current intensity of 500 mA, supporting electrolyte of 400 mg L^{-1}, and a temperature of 20°C. As shown in Fig. 6, the increase in the reaction time could increase the oil removal efficiency and decrease current efficiency. The highest efficiency of removal in reaction time of 60 min was equal to 99.77% and 99.59% using aluminum and stainless steel, respectively. However, the highest current efficiency was obtained by each of the electrodes in the 15 min. This was due to the significant reduction in COD concentration at this time. With the increasing of reaction time and decreases in the COD removal rate, the current

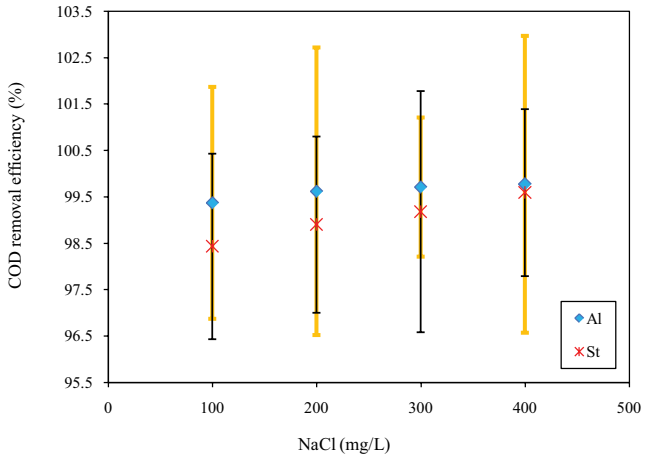

Fig. 5. COD removal rates at various supporting electrolyte concentrations (current density: 12.5 mA cm^{-2}, pH: 7, and reaction time: 60 min).

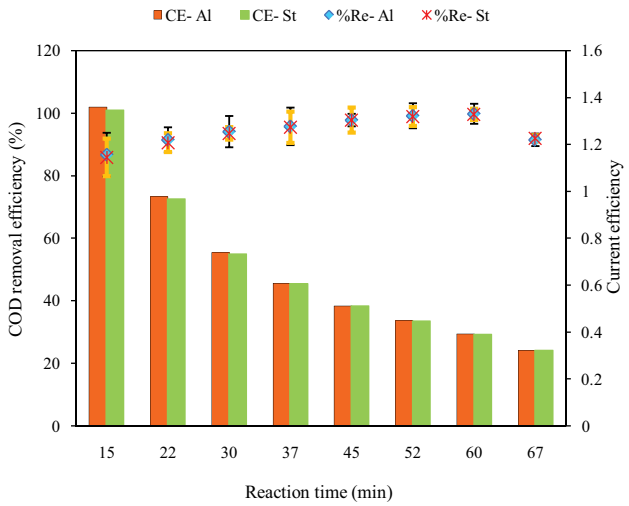

Fig. 6. COD removal rates at various reaction times (current density: 12.5 mA cm^{-2}, pH: 7, NaCl: 400 mg L^{-1}, and reaction time: 60 min).

efficiency values were decreased [14]. Since the amount of voltage and the energy consumption were increased with the reaction time, the optimum time was proposed to be 60 min.

3.5. Adsorption kinetics studies

In this study, IPD was evaluated as an adsorption kinetic model [20,21]. Also, the simplified kinetic models including the pseudo-first and second-order models were evaluated.

The linearized form of the IPD equation has been widely used to analyze the kinetics of adsorption, which calculated the following equation [22]:

$$q_t = k_p t^{1/2} + C \tag{5}$$

where q_t (mg g^{-1}) refers to the amount of oil adsorbed (as COD) at equilibrium status and time t, C is related to the intercept, and k_p (mg g^{-1}) is the rate constant of intraparticle diffusion. The present study aims to evaluate the removal of oil as COD from oily wastewater and study kinetics of reactions that occurred by an electrochemical process.

The results showed that the correlation coefficient (R^2) in this kinetic model were 0.98 and 0.97 for stainless steel and aluminum electrodes, respectively, which were less than the R^2 of second-order model (Table 1). However, these amounts of R^2 for IPD model were significant and it can be found that the IPD model can appropriately explain olive oil adsorption in the EC process. By this model, the adsorption kinetic can be evaluated at various times. Generally, adsorption mechanism can be divided into the following steps:

- Solution transfer
- Penetration of the liquid film around the solid particles into the boundary layers
- Liquid diffusion through pores of the solid surface or internal penetration
- Adsorption and desorption on internal surface places

As a result, the time required to contact the adsorbent and olive oil in the boundary layer increases. Under such conditions, the rate of pollutant diffusion through pores of the adsorbent promotes [23,24]. In this research, initially, 4,592.55 mg g^{-1} of Al-electrode was scarified and adsorbed in flocks. It was observed that, in the beginning, absorption capacity is high and the number produced flocks and removal efficiency increases over time. In the proposed electrochemical process, the pollutant is maximum at the start of the reaction and there are fewer flocks as an adsorbent. Adsorption of a contaminant onto the internal pores of the flock is done more quickly. According to this electrochemical process, the electrodes that follow this model have less corrosion, produce less flock, and have a higher removal efficiency; thus, less sludge is produced. Initial adsorption factor (R_i) for steel and aluminum were obtained as 0.27 and 0.26, respectively. These amounts show the occurrence of strong initial adsorption (Table 2). R_i was low in the early steps, suggesting a high absorption in the initial moment. With the passage of time, R_i increased and adsorption on flacks decreased. Therefore, the adsorption rate decreases with reducing the concentration of pollutants. Factors such as adsorbent particle size, solute, and contaminant physiochemical characteristics also affect the R_i values [11,25,26].

The adsorption kinetics can be formulated as:

$$q_t = \frac{V\left(\mathrm{COD}_0 - \mathrm{COD}_t\right)}{m} \tag{6}$$

where q_t refers to the quantity of oil (as COD) adsorbed at time t, m is the weight of electrode dissolved, V corresponds to the taken volume of effluent, and COD_t is COD associates with time "t." Pseudo-first and second-order kinetics models were used for quantifying the uptake kinetics. The kinetic equation is based on three assumptions:

- Sorption only occurs in the localized sites and involves no interaction between the sorb ions.

Table 1
Adsorption constants for pseudo-first-order, pseudo-second-order, and intra-particle diffusions

Type of electrode		Stainless steel	Aluminum
C_0 (mg L^{-1})		17,553	17,553
q_{exp} (mg g^{-1})		21,851.78	38,935.78
Pseudo-first-order	q_{cal} (mg g^{-1})	10,778.19	17,618
	k_1 (min^{-1})	0.0752	0.0736
	R^2	0.95	0.93
Pseudo-second-order	q_{cal} (mg g^{-1})	25,000	40,000
	k_2 (g mg^{-1} min^{-1})	0.00005	0.00003
	h (mg g^{-1} min^{-1})	23,875.01	45,479.84
	R^2	0.99	0.99
Intra-particle diffusion	k_p (mg g^{-1} $min^{0.5}$)	838.67	1,393.1
	C	15,782	28,801
	R_i	0.27	0.26
	C/q_{ref}	0.72	0.73
	R^2	0.98	0.97

Table 2
R_i and kinetic behavior according to IPD

R_i	Initial point of kinetic curve (C/q_{ref})	Initial adsorption behavior	Zone
$R_i = 1$	$C/q_{ref} = 0$	No initial adsorption	0
$0.3 > R_i > 0.9$	$0 < C/q_{ref} < 0.1$	Weakly initial adsorption	1
$0.9 > R_i > 0.5$	$0.1 < C/q_{ref} < 0.5$	Intermediately initial adsorption	2
$0.5 > R_i > 0.1$	$0.5 < C/q_{ref} < 0.9$	Strongly initial adsorption	3
$R_i < 0.1$	$C/q_{ref} > 0.9$	Approaching completely initial adsorption	4

- The energy of adsorption does not depend on surface coverage.
- Maximum adsorption corresponds to a saturated monolayer of adsorbates on the adsorbent surface [27].

The pseudo-first-order model for this propose can be generally given by [28]:

$$\ln\left(q_e - q_t\right) = \ln\left(q_e\right) - k_1 t \tag{7}$$

where q_e and q_t refer to the quantity of oil, as COD (mg g^{-1}) adsorbed at time of equilibrium and time t (h), respectively, and k_1 (min^{-1}) is the rate constant of pseudo-first-order sorption at equilibrium. In the case of many adsorption processes, the experimental kinetics data do not fit into the pseudo-first-order model over the entire range of contact time but this model can be appropriately used for their initial stages [27]. Furthermore, the pseudo-second-order model can be written as [29]:

$$\frac{t}{q_t} = \frac{1}{Kq_e^2} + \frac{1}{q_e} t \tag{8}$$

where k_2 is the pseudo-second-order rate constant (g mg^{-1} min^{-1}). Experimentally, the parameters of these models (first and second-order) can be determined by plotting $\log(q_e - q_t)$ vs. t, (t/q_t) vs. t, $1/q_t$ vs. $1/t$, q_t, and q_t/t vs. q_t [30].

or

$$\frac{q_t}{t} = \frac{h}{1 + kq_e^2} \tag{9}$$

where h can be regarded as the initial sorption rates as q_t/t when t approaches 0. Hence,

$$h = kq_e^2 \tag{10}$$

The assumptions of the pseudo-second and pseudo-first-order kinetics models are almost the same. In general, it is observed that IPD occurs through three well-differentiated steps (i) external mass transfer: the adsorbate diffuses from the solution phase to the external surface of the adsorbent, (ii) intra-particle diffusion (IPD): the adsorbate diffuses via the pores that are located at the external surface of the adsorbent and reach the adsorption sites, and (iii) rate of adsorption of the adsorbate on an active site: an equilibrium status between the solute molecules in the solution and on the adsorbent holds, instantaneously. Therefore, the number of solute molecules adsorbed onto the pores is at equilibrium with the concentration of the solute in the solution. Under such conditions, the global adsorption

rate would be controlled by external transfer and/or IPD, largely. The well-designed adsorption systems are highly efficient and present a high-quality and recyclable effluent after treatment. Moreover, if low-cost adsorbents or adsorbent regeneration is possible then the adsorbent material cost can be lowered [24]. It is therefore inferred that the unraveling adsorption kinetics of wastewater treatment should be concerned since it reveals some insights about the involved reaction pathways and adsorption mechanisms. Moreover, adsorption kinetics describes the rate of solute uptake, which controls the residence time of the adsorbate at the interface of the solid-solution. Consequently, it is of paramount importance to predict the rate of pollutant removal from aqueous solutions to design suitable plants of sorption treatment. In this study, IPD, pseudo-first-order, and pseudo-second-order models were evaluated.

3.5.1. Pseudo-first-order model

The pseudo-first-order model can be linearized as [31]:

$$\log\left(q_e - q_t\right) = \frac{\log q_e - k_1 t}{2.303} \tag{11}$$

The graph of $\log(q_e - q_t)$ vs. t, can be employed to determine k_1 and q_e as the slope and intercept of the plot, respectively (Table 1). The pseudo-first-order model shows that the kinetics of diffusion is monolayer and adsorption depends on the adsorbent capacity. In the EC/EF process, corrosion of the anode, and generation of hydroxide flock plays the adsorbent role. In this model, adsorption values vs. time are directly related to the number of unoccupied sites on the adsorbent [32]. In a typical adsorbent, pollutant adsorption rate is high at the initial stage of the process, because there are many adsorption sites available and pollutant is adsorbed more quickly. However, with the course of time, the rate of pollutant adsorption is reduced. In comparison, in the electrochemical processes, the coagulant is produced constantly and, hence, compared with conventional absorbents, there would not be a considerable decrease in the absorption rate. As the results illustrate, experimental data did relatively conform to a linear plot, with 0.93 and 0.95 being correlation coefficients for the Al and St electrodes, respectively. Thus, the reaction could be classified as pseudo-first-order.

3.5.2. Pseudo-second-order model

The pseudo-second-order model can be linearized as [33]:

$$\frac{t}{q_t} = \frac{1}{\left(k_2 q_e^2\right)} + \frac{t}{q_e} \tag{12}$$

where k_2 is the rate constant of second-order adsorption (g μg^{-1} min), and q_e refers to the adsorption capacity, which can be calculated through the pseudo-second-order kinetic model ($\mu g\ g^{-1}$). The k_2 and q_e values can be, respectively, determined based on the slope and intercept of a plot of t/q_t vs. t. The kinetics model of pseudo-second-order indicates that the chemical adsorption is a slow process that is controlled by the surface adsorption processes. This model relies on solid-phase adsorption where the number of occupied adsorption sites is proportional to the square of the number of unoccupied sites. The results exhibit that the experimental data completely conform to a linear plot with a high correlation coefficient (Table 1). Hence, the reaction could be classified as the pseudo-second-order and this kinetics model can be adopted to explain adsorption of oil as COD in the EC process, appropriately. These results imply the assumption that chemisorption is the rate-limiting step is valid, where the chemisorption process is due to valence forces caused by the exchange or sharing of electrons between the adsorbent and metal ions.

3.6. Characterization of the sludge obtained from the EC process

Through the experiments, a brown sediment was produced on the surface and bottom of the reactor. Since oil is lightweight, sludge accumulation on the reactor surface was more noticeable than its bottom. Also, hydrogen bubbles generated in the reactor were very effective against flock flotation. During the reaction, the generation of hydroxyl radicals caused oxidation and breakdown of the oil's carbon chain. Broken materials were entrapped in the flock generated in the anodes and were eliminated from the liquid. The sludge produced in the EC process separated from the solution and dried for 3–4 h in an oven. The X-ray fluorescence (XRF) and Fourier-transform infrared spectroscopy (FTIR) analyses were performed on the sludge samples. The obtained results from XRF analyzes were showed that the elements of Zn, Cu, and Cl and the elements of Cl and Cr were presented in the sludge of aluminum and steel electrodes, respectively (Table 3). Moreover, there metal oxides such as Fe_2O_3 were produced in the both electrodes. The amount of amount was higher than the aluminum electrodes. The result can be attributed to the nature of the electrodes.

The major constituents from a loss on ignition (LOI) were measured to be 74.27% and 66.52% for anode-Al and

Table 3
XRF analysis results of sludge produced during the EC process

Parameters	Anode – Al (%)	Anode – St (%)
L.O.I	74.27	66.52
Na_2O	0.738	0.9
MgO	0.063	0.026
Al_2O_3	18.607	–
SiO_2	0.101	0.12
P_2O_5	0.08	0.063
SO_3	5.775	5.142
Cl	0.092	0.183
CaO	0.03	–
MnO	0.079	0.111
Fe_2O_3	0.136	23.916
Cu	0.013	–
Zn	0.015	–
Cr	–	3.018

anode-St, respectively, by the mass of EC sludge. The LOI indicates the amount of organic matter in a sample that combusts at 550°C. The weight drop during combustion is equal to the sample's weight of organic matter. It means that 74.27% and 66.52% of the EC sludge are respectively an organic matter or volatile solids content as the mass of the sludge can be reduced by incineration. The content of volatile solids is usually quoted as a weight percentage of the total solid residues. The residual solids remaining after ignition is called as the fixed residue, which defines the weight of inorganic content of the sludge, that is, the mass of solids that remains for ultimate disposal after the incineration. As presented in Table 3, anode-Al flocks formed into Al_2O_3 while small amounts of Fe_2O_3 formed into anode-St. However, only Fe_2O_3 formed a flock. The structure of sludge after treating the oily wastewater by the electrochemical method was analyzed by FTIR. As shown in Fig. 7, the peaks were obtained at 460.36 to 2,924.80, which represents breaking the oil's 18-carbon chains and turning it into by-products. This breakdown, as an outcome of the reaction, may happen due to the presence of the hydroxyl radicals. Alkane's wavelengths above 2,000 further indicate that $–CH_2–$ is caged by the flocks. Ketones, amides, amines, esters, and alcohols were detected at a lower wavelength. In general, the electrochemical process is inferred as a process that creates free radicals in the solution and breaks the carbon chain of oil. Byproducts generated in the solution adhere to the flock and finally precipitate or transfer to the surface by hydrogen bubbles at the cathode. If IPD is involved in the mechanism of adsorption, plotting the square root of time against the adsorption (q_t) would result in a linear relationship. Therefore, IPD would be the controlling stage if this line passes through the origin of the plot.

$$q = k_p t^{0.5} \tag{13}$$

Different slopes in the linear plot of q vs. $t^{0.5}$ obtained by piecewise linear regression implied various mechanisms of mass transfer. IPD and external mass transfer in the macro-, meso-, and microporous structures of the adsorbent correspond to different sequential phases of mass transport with a decreasing rate. This model $t^{0.5}$ vs. q_t is a multi-line graph that indicates the occurrence of two or more steps in the adsorption process [24].

$$q_{\text{ref}} = k_p t_{\text{ref}}^{1/2} + C \tag{14}$$

$$q_{\text{ref}} - q_t = k_p \left(t_{\text{ref}}^{1/2} - t^{1/2} \right) \tag{15}$$

$$\left(\frac{q_t}{q_{\text{ref}}} \right) = 1 - R_i \left[1 - \left(\frac{t}{t_{\text{ref}}} \right)^{1/2} \right] \tag{16}$$

$$R_i = \frac{t_{\text{ref}} - C}{t_{\text{ref}}} = 1 - \left(\frac{C}{q_{\text{ref}}} \right) \tag{17}$$

Eq. (17) expresses R_i as the ratio of the amount of initial adsorption (C) to the amount of final adsorption (q_{ref}). In the case of $C = 0$, the system does not involve initial adsorption and $R_i = 1$. However, when $C = q_{\text{ref}}$, adsorption occurs as the process initiates and $R_i = 0$ (Table 2). Treating wastewater with the electrochemical method occurs by dissolving anode as the coagulant. This coagulant possesses a high capacity of adsorbing water with metal hydroxide forms.

4. Conclusion

Based on the obtained results, the conclusions of the present study can be summarized as follows:

The optimized process resulted in removal of above 99% oily wastewater as COD, where the corresponding optimum parameters were current density (12.5 mA cm^{-2}), pH = 5 for the Al-electrode, and pH = 9 for the St-electrode, supporting electrolyte (400 mg L^{-1}), 17,500 mg L^{-1} initial COD concentration, and 60 min time. Additionally, COD adsorption in the EC process followed the pseudo-second-order and IPD kinetic model. At the initial step of the adsorption process,

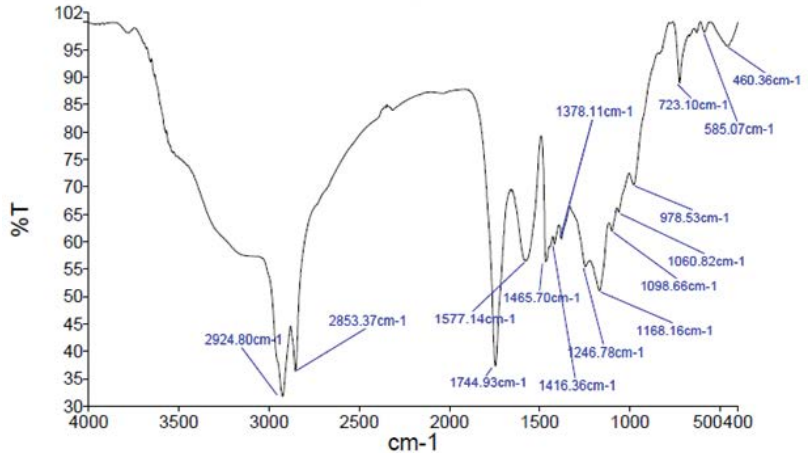

Fig. 7. FTIR of oily wastewater sludge of the electrochemical process using stainless steel and aluminum as a cathode and anode electrodes, respectively.

4,592.55 (mg L^{-1}) for Al-electrode and 4,927.4 (mg L^{-1}) for Fe-electrode (as COD) were removed and adsorbed onto the flocks, respectively. According to the IPD, at the initial time, absorption capacity is high while the produced flocks and removal efficiency increases over time. The structure of sludge after treating oily wastewater by electrochemical method was characterized by FTIR and found the breakdown of the 18-carbon chain of oil and turning it into by-products. Byproducts were formed in the solution via involvement of the flock and finally precipitated or were brought to the surface through the cathodic hydrogen bubbles.

Acknowledgment

The authors wish to acknowledge the financial support of Tarbiat Modares University.

References

[1] M. Usman, E. Salama, M. Aif, B. Jeon, X. Kaili, Determination of the inhibitory concentration level of fat, oil, and grease (FOG) towards bacterial and archaeal communities in anaerobic digestion, Renewable Sustainable Energy Rev., 131 (2020) 110032–110043.
[2] C. Gurd, R. Villa, B. Jefferson, Understanding why fat, oil and grease (FOG) bioremediation can be unsuccessful, J. Environ. Manage., 267 (2020) 110647–110657.
[3] M. Víctor-Ortega, J.M. Ochando-Pulido, G. Hodaifa, A. Martinez-Ferez, Final purification of synthetic olive oil mill wastewater treated by chemical oxidation using ion exchange: study of operating parameters, Chem. Eng. Process., 85 (2014) 241–247.
[4] M. Stoller, J.M. Ochando-Pulido, G. Vilardi, Technical and economic impact of photocatalysis as a pretreatment process step in olive mill wastewater treatment by membranes, Chem. Eng. Trans., 57 (2017) 1171–1176.
[5] K. Yuney, A.A. Oladipo, M. Gazi, CuO coated olive cake nanocomposites for rapid phenol removal and effective discoloration of high strength olive mill wastewater, Chemosphere, 253 (2020) 126703–126713.
[6] L. Cai, J. Sun, Y. Jiang, Z. Huang, Stabilization of heavy metals in piggery wastewater sludge through coagulation-hydrothermal reaction–pyrolysis process and sludge biochar for tylosin removal, J. Cleaner Prod., 260 (2020) 121165–121173.
[7] J. Akansha, P.V. Nidheesh, A. Gopinatha, K.V. Anupama, M. Suresh Kumara, Treatment of dairy industry wastewater by combined aerated electrocoagulation and phytoremediation process, Chemosphere, 253 (2020) 126652–126660.
[8] J. Dotto, M. Fagundes-Klen, M.T. Veit, S.M. Palacio, R. Bergamasco, Performance of different coagulants in the coagulation/flocculation process of textile wastewater, J. Cleaner Prod., 208 (2019) 656–665.
[9] D. Marmanis, K. Dermentzis, A. Christoforidis, Electrochemical treatment of olive mill waste powered by photovoltaic solar energy, J. Power Technol., 98 (2019) 377–381.
[10] X. Guo, J. Wang, A general kinetic model for adsorption: theoretical analysis and modelling, J. Mol. Liq., 288 (2019), doi: 10.1016/j.molliq.2019.111100.
[11] A.E. Regazzoni, E. Alberto, Adsorption kinetics at solid/aqueous solution interfaces: on the boundaries of the pseudo-second-order rate equation, Colloids Surf., A, 585 (2020), doi: 10.1016/j.colsurfa.2019.124093.
[12] S.P. Kuang, Z. Wang, J. Liu, Preparation of triethylene-tetramine grafted magnetic chitosan for adsorption of Pb(II) ion from aqueous solutions, J. Hazard. Mater., 260 (2013) 210–219.
[13] E.E. Gerek, S. Yılmaz, A. Savaş Koparal Combined energy and removal efficiency of electrochemical wastewater treatment for leather industry, J. Water Process Eng., 30 (2019), doi: 10.1016/j.jwpe.2017.03.007.
[14] J.B. Parsa, M. Rezaei, A. Soleymani, Electrochemical oxidation of an azo dye in aqueous media investigation of operational parameters and kinetics, J. Hazard. Mater., 168 (2009) 997–1003.
[15] F. Ghanbari, M. Moradi, A comparative study of electrocoagulation, electrochemical Fenton, electro-Fenton and peroxi-coagulation for decolorization of real textile wastewater: electrical energy consumption and biodegradability improvement, J. Environ. Chem. Eng., 3 (2015) 499–506.
[16] A. Sharm, Z. Syed, U.B. Akhilend, B. Gupta, C. Ram, Adsorption of textile wastewater on alkali-activated sand, J. Cleaner Prod., 220 (2019) 23–31.
[17] L.M.A. Fayoumi, M.A. Ezzedine, H.H. Akel, M.M.E. Jamal, Kinetic study of the degradation of crystal violet by $K_2S_2O_8$ comparison with malachite green, Portugaliae Electrochim. Acta, 30 (2012) 121–133.
[18] N. Flores, E. Brillas, F. Centellas, R.M. Rodríguez, P.L. Cabot, J.A. Garrido, I. Sirés, Treatment of olive oil mill wastewater by single electrocoagulation with different electrodes and sequential electrocoagulation/electrochemical Fenton-based processes, J. Hazard. Mater., 347 (2018) 58–66.
[19] K. Szewczuk-Karpis, M. Wisniewsk, Adsorption layer structure at soil mineral/biopolymer/supporting electrolyte interface – the impact on solid aggregation, J. Mol. Liq., 284 (2019) 117–123.
[20] H.M. Jang, S. Yoo, Y.K. Choi, S. Park, E. Kan, Adsorption isotherm, kinetic modeling and mechanism of tetracycline on *Pinus taeda*-derived activated biochar, Bioresour. Technol., 259 (2018) 24–31.
[21] S. Jiang, T. Yu, R. Xia, X. Wang, Realization of super high adsorption capability of 2D δ-MnO_2/GO through intra-particle diffusion, Mater. Chem. Phys., 232 (2019) 374–381.
[22] N.A. Akbar, N.M. Kamil, H. Aziz, Assessment of kinetic models on Fe adsorption in groundwater using high-quality limestone, IOP Conf. Ser.: Earth Environ. Sci., 49 (2018), doi: 10.1088/1755-1315/140/1/012030.
[23] S. Jiang, T. Yu, R. Xia, X. Wang, M. Gao, Realization of super high adsorption capability of 2Dδ-$MnO_2^{\bullet}$/GO through intra-particle diffusion, Mater. Chem. Phys., 232 (2019) 374–381.
[24] F.C. Wu, R.L. Tseng, R.S. Juang, Initial behavior of intraparticle diffusion model used in the description of adsorption kinetics, Chem. Eng. J., 153 (2009) 1–8.
[25] J.P. Simonin, On the comparison of pseudo-first-order and pseudo-second-order rate laws in the modeling of adsorption kinetics, Chem. Eng. J., 300 (2016) 254–263.
[26] R.K. Khamizov, D.A. Sveshnikova, A.E. Kucherova, L.A. Sinyaeva, Kinetic model of batch sorption processes: comparing calculated and experimental data, Russ. J. Phys. Chem. A, 10 (2018) 2032–2038.
[27] J.D. Méndez-Díaz, G. Prados-Joya, J. Rivera-Utrilla, R. Leyva-Ramos, M. Sánchez-Polo, M.A. Ferro-García, N.A. Medellín-Castillo, Kinetic study of the adsorption of nitroimidazole antibiotics on activated carbons in aqueous phase, J. Colloid Interface Sci., 345 (2010) 481–490.
[28] Y.A. Ouaissa, M. Chabani, A. Amrane, Removal of tetracycline by electrocoagulation: kinetic and isotherm modeling through adsorption, J. Environ. Chem. Eng., 2 (2014) 177–184.
[29] S. Salvestrini, Analysis of the Langmuir rate equation in its differential and integrated form for adsorption processes and a comparison with the pseudo-first and pseudo-second-order models, React. Kinet. Mech. Catal., 123 (2018) 455–472.
[30] Y. Xiao, J. Azaiez, J.M. Hill, Erroneous application of pseudo-second-order adsorption kinetics model: ignored assumptions and spurious correlations, Ind. Eng. Chem. Res., 57 (2018) 2705–2709.
[31] D. Robati, Pseudo-second-order kinetic equations for modeling adsorption systems for removal of lead ions using multi-walled carbon nanotube, J. Nanostruct. Chem., 3 (2013) 1–6.
[32] G. Yuvaraja, N. Krishnaiah, M.V. Subbaiah, A. Krishnaiah, Biosorption of Pb(II) from aqueous solution by *Solanum melongena* leaf powder as a low-cost biosorbent prepared from agricultural waste, Colloids Surf., B, 114 (2014) 75–81.
[33] F. Deniz, Potential use of shell biomass (*Juglans regia* L.) for dye removal: relationships between kinetic pseudo-second-order model parameters and biosorption efficiency, Desal. Water Treat., 52 (2014) 1–3.